Kinetic Studies of Polyhydroxybutyrate Granule Formation in *Wautersia eutropha* H16 by Transmission Electron Microscopy

Jiamin Tian,[1] Anthony J. Sinskey,[2] and JoAnne Stubbe[1,2]*

Department of Chemistry[1] and Department of Biology,[2] Massachusetts Institute of Technology, 77 Massachusetts Avenue, Cambridge, Massachusetts 02139

Wautersia eutropha, **formerly known as** *Ralstonia eutropha*, **a gram-negative bacterium, accumulates polyhydroxybutyrate (PHB) as insoluble granules inside the cell when nutrients other than carbon are limited. In this paper, we report findings from kinetic studies of granule formation and degradation in** *W. eutropha* **H16 obtained using transmission electron microscopy (TEM). In nitrogen-limited growth medium, the phenotype of the cells at the early stages of granule formation was revealed for the first time. At the center of the cells, dark-stained "mediation elements" with small granules attached were observed. These mediation elements are proposed to serve as nucleation sites for granule initiation. TEM images also revealed that when** *W. eutropha* **cells were introduced into nitrogen-limited medium from nutrient-rich medium, the cell size increased two- to threefold, and the cells underwent additional volume changes during growth. Unbiased stereology was used to analyze the two-dimensional TEM images, from which the average volume of a** *W. eutropha* **H16 cell and the total surface area of granules per cell in nutrient-rich and PHB production media were obtained. These parameters were essential in the calculation of the concentration of proteins involved in PHB formation and utilization and their changes with time. The extent of protein coverage of the granule surface area is presented in the accompanying paper (J. Tian, A. He, A. Lawrence, P. Liu, N. Watson, A. J. Sinskey, and J. Stubbe, J. Bacteriol. 187:3825–3832, 2005).**

Polyhydroxyalkanoates (PHAs), which are polymers composed of polyoxoesters, are accumulated in granular form by various microorganisms under nutrient-limited conditions when a carbon source is readily available (1). They serve as reserves of carbon and reducing equivalents to preserve cell survival during stressful conditions. Little do these bacteria know that their biodegradable PHAs have properties ranging from thermoplastics to elastomers and could potentially replace the nonenvironmentally friendly petroleum-based plastics that are heavily used in our society. Production of economically competitive PHAs and PHAs with new properties has been the impetus for many research groups to study the biosynthesis, degradation, and homeostasis of PHAs in microorganisms. Biosynthesis of PHAs involves transforming soluble substrates, such as hydroxyalkanoate coenzyme A esters, into insoluble inclusions during polymer elongation; these inclusions are stored in a form that can be rapidly degraded when necessary (28).

In an effort to elucidate the mechanism of PHA biosynthesis and degradation, various research groups have identified important proteins that play a role in these processes (14, 20, 24, 27, 29, 37, 38). *Wautersia eutropha*, the most extensively studied microorganism, uses 3′-hydroxybutyryl coenzyme A to make polyhydroxybutyrates (PHBs). To maximize the production of PHBs, *W. eutropha* is typically grown in nitrogen-limited medium with an available carbon source such as fructose (PHB

production medium [PHB$_P$]) (38). At late stages of PHB accumulation, the polymer can account for 80 to 85% of the dry cell weight. Transmission electron microscopy (TEM) and immunogold labeling experiments with preparations examined by TEM at a late stage of PHB production have revealed that the entire inside of each cell is filled with 8 to 12 PHB granules that are 0.2 to 0.5 μm in diameter (1). The synthase (PhaC) and phasin (PhaP) proteins were shown to be located on the granule surface (15, 22, 27). The extent of coverage by PhaC is low, while the extent of coverage by PhaP is substantially higher. Early electron microscopy studies of PHB granules from *Bacillus cereus*, *Bacillus megaterium* (23), *Rhodospirillum rubrum* (3), and *Chlorogloea fristschii* (19) all revealed an atypical membrane-like material surrounding the surface of granules, which varied in thickness from 3 nm to 20 nm depending on the species. Recent atomic force microscopy studies of granules freshly isolated from *W. eutropha* with minimum perturbation also demonstrated that there was a 3- to 4-nm-thick boundary layer surrounding the surface of the granules (7). In addition, globular structures, which were 35 nm in diameter with a central pore, were also reported to be on the surface of the granules and were proposed to be centers for PHB synthesis and depolymerization. Based on these observations, two models have been proposed for granule formation. The first model is the micelle model, in which the extended PHB chains covalently attached to the synthase aggregate initially into a micelle structure (Fig. 1) (12, 14). The physical properties of the polymer are thus proposed to be the driving force for inclusion formation. The second model is the budding model that we proposed recently, in which the hydrophobic synthase binds to the inner face of the plasma membrane and buds from this

* Corresponding author. Mailing address: Bldg. 18-598, Department of Chemistry, Massachusetts Institute of Technology, 77 Massachusetts Ave., Cambridge, MA 02139. Phone: (617) 253-1814. Fax: (617) 258-7247. E-mail: stubbe@mit.edu.
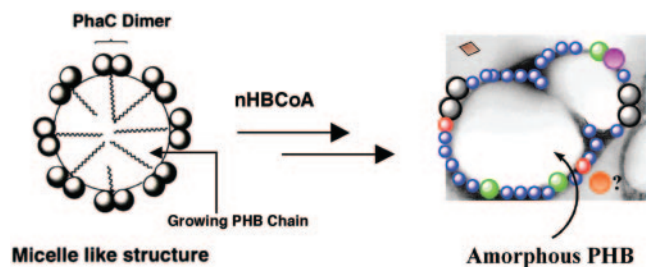
FIG. 1. Granule formation through micelle formation from hydroxybutyrate chains covalently attached to PhaC. The colored spheres shown on amorphous PHB represent proteins that have been shown to or are proposed to associate with the granule surface. Gray spheres, PhaC; blue spheres, PhaP; red spheres, PhaR; green spheres, PhaZ1$_a$; purple sphere, PhaZ1$_b$; orange sphere, PhaZ1$_c$; brown diamond, oligomer hydrolase. nHBCoA, hydroxybutyryl coenzyme A.

membrane, leading to a granule surface covered with a lipid monolayer (Fig. 2) (32). In this model, the biology of the system and the physical properties of the polymer both are required for granule formation.

Our lab has been interested in the mechanism of granule formation and degradation. Studying granule formation from its inception (that is, the early stage of PHB biosynthesis) has not previously been reported and may allow a distinction between the two models (Fig. 1 and 2). In the present study, TEM was used to study the kinetics of granule formation and degradation in *W. eutropha* H16. The TEM images of cells at the early stages of PHB production revealed dark-stained mediation elements near the center of the cell, ringed by small granules (≤0.1 μm in diameter). These images led to an alternative model for granule formation, in which granules are localized and the new mediation elements function as granule initiation sites. In addition, the time course studies revealed changes in cell and granule sizes, which were quantitatively analyzed by unbiased stereology. Stereology, a branch of ap-

plied mathematics, is the three-dimensional interpretation of flat images by criteria of geometric probability (10). Using this analysis method, we report for the first time the average volume of *W. eutropha* H16 cells and the total surface area of granules per cell at different stages of granule formation. These parameters, along with the results of quantitative Western analyses described in the accompanying paper (34), identified the proteins involved during PHB biosynthesis and degradation and the changes in concentration of these proteins as a function of time. The kinetic information is essential for proposing functional roles of the proteins in PHB homeostasis.

MATERIALS AND METHODS

Cultivation conditions. Wild-type *W. eutropha* H16 was cultivated with aeration at 30°C. Gentamicin was included in all growth media, except when PHB utilization was being measured. A single colony from a dextrose-free tryptic soy broth (TSB) (Becton Dickinson Microbiology Systems, Cockeysville, MD) plate was cultivated in 5 ml of TSB to saturation (~40 h), at which time 2 ml was transferred into 100 ml of TSB in 500-ml baffled flasks and grown for 24 h. The doubling time of *W. eutropha* H16 in TSB is between 3 and 4 h. Cells harvested by centrifugation were washed and transferred into 200 ml of TSB or 200 ml of PHB$_P$ (minimal medium supplemented with 1% fructose and 0.01% [wt/vol] ammonium chloride) in 1-liter baffled flasks to obtain cultures with an initial optical density at 600 nm of 0.5. For cells grown under TSB conditions, 5 ml of cells was removed at 4 and 24 h for TEM analysis. For cells grown in PHB$_P$, 5 ml of cells was removed from the culture at 2.5, 5, 9, 24, and 73 h. In all cases, cells were immediately fixed for TEM studies. For PHB utilization, 100 ml of cells grown in PHB$_P$ for 73 h was harvested, washed with 0.85% (wt/vol) saline, and transferred into 200 ml of PHB utilization medium (PHB$_U$) (minimal medium supplemented with 0.5% [wt/vol] ammonium chloride). Samples were harvested at 48 h for TEM analysis.

Reagents. All TEM reagents were purchased from Electron Microscopy Sciences (Hatfield, PA).

Fixation. Five milliliters of the cell culture in TSB, PHB$_P$, or PHB$_U$ at various times was transferred to a 15-ml Falcon tube containing 5 ml of fresh fixative solution (2% [vol/vol] glutaraldehyde, 3% [wt/vol] paraformaldehyde made fresh, 5% [wt/vol] sucrose, and 0.1 M sodium cacodylate buffer, pH 7.4). After 5 min of manual mixing, the cells were spun down at 5,000 rpm for 10 min using a bench centrifuge. The supernatant was removed, and an additional fresh 10 ml of the fixative solution was added to resuspend the cell pellet. After 1 h of incubation at room temperature with occasional manual mixing, the cells were pelleted
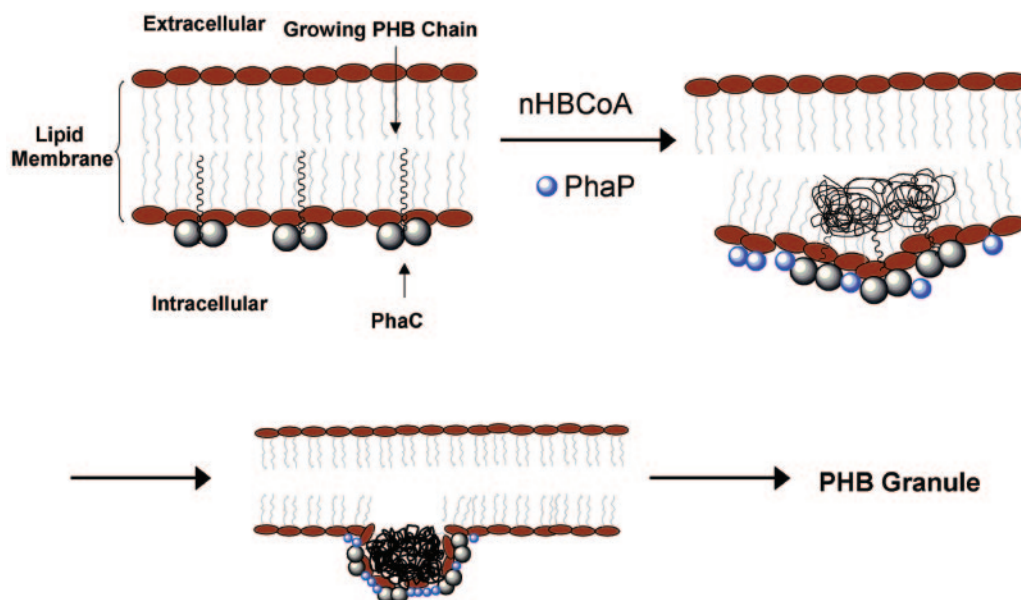

FIG. 2. Granule formation through budding from the inner leaflet of the plasma membrane. nHBCoA, hydroxybutyryl coenzyme A.

again. Sodium cacodylate buffer (0.1 M at pH 7.4; 1.5 ml) was added to resuspend the pellet. The cell suspension was transferred to an Eppendorf tube (1.7 ml), and after 2 min of mixing, the cells were spun down at 9,000 rpm for 1 min in a minicentrifuge. The supernatant was removed, and the pellet was washed three times with 1.5 ml of 0.1 M sodium cacodylate buffer. The pellet was dislodged from the bottom of the Eppendorf tube to ensure good washing each time.

The cell pellet was then fixed with 1.5 ml of a 1% osmium solution prepared by mixing 1.25 ml of 4% osmium tetroxide (OsO_4) (Electron Microscopy Sciences), 1 ml of 0.1 N HCl, 1.75 ml of distilled H_2O, and 1 ml of acetate-Veronal stock (1.2% [wt/vol] anhydrous sodium acetate and 2.9% [wt/vol] sodium barbituate [Veronal] in distilled H_2O). The pellet was dislodged from the bottom of the tube and incubated in the osmium solution for 1 h.

The fixed cells were then pelleted, and 1.5 ml of a third fixative solution, the Kellenberger uranyl acetate solution (0.5% [wt/vol] uranyl acetate in Veronal-acetate buffer) was added. The pellet was initially washed with this solution briefly (<1min) and then incubated in 1.5 ml of fresh solution overnight in the dark.

Dehydration. Upon the completion of uranyl acetate staining, the pellet was rinsed with ~1.5 ml of distilled H_2O quickly after being dislodged and was then pelleted by centrifugation. To dehydrate the cells, they were subjected to increasing amounts of ethanol. The pellet was placed first in 50% (vol/vol) ethanol-water for 10 min and subsequently in 70% (vol/vol) ethanol for 10 min, 95% (vol/vol) ethanol for 10 min, and then three times in 100% ethanol for 15 min. The cells were spun down after each ethanol treatment to remove the supernatant, and the pellet was dislodged during each incubation to ensure homogeneous dehydration. The pellet was further dehydrated in 50% (vol/vol) ethanol-50% (vol/vol) propylene oxide for less than 5 min before it was transferred to 100% propylene oxide (~1.5 ml). After 5 min, the pellet was then placed in 50% propylene oxide–50% low-viscosity embedding resin (containing vinyl-4-cyclohexene dioxide, DER 736 resin, nonenyl succinic anhydride, and 2-dimethylaminoethanol; these components were mixed in proportions to obtain hard blocks when the instructions of a Spurr kit were followed) and rotated on a rotator for 12 h.

Embedding. All of the pellet was transferred into ~1.5 ml of 100% low-viscosity embedding resin and placed under a vacuum in a desiccator for 4 h. This process was repeated at least three times with fresh embedding resin. The pellet was then cut into small sections randomly and embedded in beam capsules containing 100% low-viscosity embedding resin. The beam capsules were then placed at 60°C overnight to allow embedding.

Sectioning and microscopy. Ultrathin sections (thickness, ~70 nm) were cut with a Reichert Ultracut E microtome using a Diatome diamond knife. The sections were picked up with 200-mesh nickel grids coated with Formvar (0.3% [wt/vol] dissolved in ethylene dichloride) and a layer of carbon. Serial sections were also prepared for wild-type *W. eutropha* cells grown in PHB_P for 5 h. The thickness of each section was ~70 nm. The sections were examined using a Philips EM410 or JOEL JEM-1200EXII electron microscope at 80 kV. For each condition, images were recorded on film at high and low magnifications.

TEM image data analysis: calculation of the average cell volume at 5 h of the wild-type strain grown in PHB_P. *W. eutropha* cells appear to be rod shaped under a light microscope, and all calculations of volumes are based on this premise. Thus, the volume of a cell has been approximated by using the equation describing the volume of a cylinder: $V_C = \pi d^2 h/4$, where V_C is the volume of a cylinder or a single cell, d is the diameter of the cylinder or the width of the cell, and h is the height of the cylinder or the length of the cell. Serial sections (~70 nm; 5 h in PHB_P) were required to obtain the actual length and width of a cell by selecting the longest and widest cell profiles, respectively, in images. Here, cell profiles refer to the cross section of cells resulting from a single cut. Long cell profiles that did not change length and angle from one section to the next were measured with a ruler to determine the length (h); similarly, wide cell profiles that did not change width and angle from one section to the next were measured to determine the width (d). All measured values were corrected by the magnification factor. The average cell volume for this sample is referred to here as V_{C5h}. This analysis assumed that the cells were uniform in size at this time, which was not the case. At 5 h under the growth conditions used, the cells were dividing. Since the analysis involved examination of successive sections for the longest cells which were on the verge of dividing, V_{C5h} was the average cell volume at this stage. The average cell volume of freshly divided cells at 5 h was assumed to be one-half of V_{C5h}. Thus, as noted in Table 1, a range of volumes is reported here for the times at which cells were dividing. In the stationary phase (TSB at 24 h and PHB_P at 9 to 73 h), the cells were assumed to be uniform.

Calculation of the area of cell profiles on two-dimensional (2-D) images using

TABLE 1. Estimated average cell volume and total surface area of granules per *W. eutropha* H16 cell determined by the stereology method and reported as a function of time and cultivation conditions[a]

Sample	A_{CP}/N_{CP} (μm^2)[b]	CE (%)[c]	V_C (μm^3)[d]	S_G (μm^2)[e]
TSB, 4 h[f]	0.84	8	0.9–1.8	1.3–2.5
TSB, 24 h	0.42	6	0.9	1.3
PHB_P, 2.5 h[f]	1.09	6	1.2–2.3	ND[g]
PHB_P, 5 h[f]	0.82	5	0.9–1.8	ND[g]
PHB_P, 9 h	0.50	10	1.1	3.6
PHB_P, 24 h	0.55	8	1.2	7.3
PHB_P, 73 h	0.64	9	1.4	11.2[h]
PHB_U, 48 h	0.49	4	ND[i]	ND[i]

[a] The change in cell volume is also reflected in the A_{CP}/N_{CP} values. Note that the coefficient of error associated with A_{CP}/N_{CP} is also the minimum coefficient of error associated with V_C.
[b] Total area of cell profiles/number of cell profiles.
[c] CE, coefficient of error. The sampling error associated with A_{CP}/N_{CP} also applies to V_C.
[d] Average volume of a cell.
[e] Average total surface area of granules per cell.
[f] Cells are dividing at these times; ranges of V_C and S_G are shown.
[g] ND, not determined since granules were too small and ill defined.
[h] The tiny granules observed at this time were also counted during measurement.
[i] ND, not determined since there seemed to be different phenotypes of cells.

unbiased stereology at different times. The Cavalieri point counting method was used to calculate the area of cell profiles (5, 26). A multipurpose test system was used. The probe contained parallel lines (also called test lines) spaced 19.85 mm apart and points spaced 39.7 mm apart evenly on each line (http://web.mit.edu/biochemistry/PHB_Supp_1.pdf). The probe was overlaid randomly on a TEM image containing cell profiles. The number of points (P) that hit cell profiles was then tabulated. This process was repeated with images of other random sections of the same sample until enough points were obtained so that the coefficient of error was less than 10%. The coefficient of error, also known as sampling error, is defined as follows: (standard deviation/mean)/(sample number)$^{1/2}$, where the sample number is equal to the number of images used for the study. Typically, a minimum of 100 to 200 points is needed. The area of the cell profiles covered in all images was calculated using equation 1 (16, 33).

$$A_{CP} = \Sigma P_{CP} \times a(p) \qquad (1)$$

where A_{CP} is the total area of the cell profiles on all images, ΣP_{CP} is the number of points hitting the cell profiles, summed over all images, and $a(p)$ is the area per point, the product of the distances between points in the x and y directions (19.85 mm by 39.7 mm). Since all images were magnified, $a(p)$ was corrected by the magnification factor.

Calculation of the average volume of cells at each time using A_{CP} of the corresponding sample and V_{C5h}. The Delesse principle states that the two-dimensional (2-D) areas of profiles of tissue components are related to the three-dimensional volumes occupied in space by these components, assuming random distribution and random orientation of components (6). The relationship between area and volume is shown in equation 2.

$$A_A = V_V \qquad (2)$$

where A_A is the area fraction and V_V is the volume fraction. Both A_A and V_V are further defined as shown in equation 3.

$$A_A = \frac{A_{obj}}{A_{ref}} = \frac{V_{obj}}{V_{ref}} = V_V \qquad (3)$$

where A_{obj} is the area of the object of interest on flat images, which in our case was equal to the area of total cell profiles (A_{CP}) described above; A_{ref} is the area of the reference space that contained A_{obj}, which can be obtained by counting the total number of points on the point-grid probe used to obtain A_{CP} and multiplying the total number of points by the area per point (equation 1); V_{obj} is the volume of the object of interest, which in our case was the total volume of the cells observed in images from which A_{obj} was measured; and V_{ref} is the reference volume that contained V_{obj}. Since A_{CP} is a function of ΣP_{CP} (equation 1), a value that is highly dependent on the number of observed cell profiles present on TEM

images which are all taken at random, a normalization procedure is necessary in order to compare A_{CP} values calculated for samples collected at each time point. Therefore, the total number of cell profiles (N_{CP}) in all the images measured is determined. In order to avoid overcounting, a counting rule is applied. The cell profiles that lie within the reference area and only those that are on the top and at the left edge of the reference area are counted. Note that N_{CP} only refers to the total number of cell profiles that are observed and therefore contribute to the measurement of A_{CP}. Therefore, the A_{CP}/N_{CP} values obtained from different samples are indicative of the trends in volume change. When parameters of separate samples, such as 2.5-h and 5-h PHB$_P$ samples, are compared, the relationship among the A_{CP}, volume of cell profiles (V_{CP}), and N_{CP} when the thickness of each section is the same can be found in the equation 4.

$$\left(\frac{V_{CP2.5h}}{N_{CP2.5h}}\right) = \left(\frac{V_{CP5h}}{N_{CP5h}}\right) \times \frac{A_{CP2.5h}}{A_{CP5h}} \times \frac{N_{CP5h}}{N_{CP2.5h}} \qquad (4)$$

Notice that we did not chose to cancel out the $N_{CP2.5h}$ and N_{CP5h} terms in this equation. This is because the terms in the parentheses (V_{CP}/N_{CP}) now represent the actual average volume of a cell (V_C). This representation is valid only when the number of cell profiles is equivalent to the number of cells present in the reference space, which is true in our system since a cylindrical cell can appear only once when it is sliced from any angle. The only exception is when the cells are dividing. Since the middle of a cell pinches in, sectioning the cell longitudinally on the edge could result in two profiles. However, the probability of this is low (≤ 2 or 3% for ~100 cell profiles) (data not shown). In addition, cell division does not occur in PHB$_P$ at 9, 24, and 73 h. Since we obtained the actual average volume of a cell in PHB$_P$ at 5 using images of serial sections as described above, knowing $A_{CP2.5\,h}$, A_{CP5h}, $N_{CP2.5\,h}$, and N_{CP5h} allowed us to calculate the approximate average volume of a cell in PHB$_P$ at 2.5 h. Similarly, an estimate of the average volume of a cell from other samples could be obtained using this method. Equation 4 is valid when the thickness of a section is the same for different samples, which was the case for this study.

Calculation of the total surface area of granules per cell using unbiased stereology. The multipurpose test system (http://web.mit.edu/biochemistry/PHB_Supp_1.pdf) was again overlaid on TEM images of the same sample randomly (all images were the same magnification). The size of the image defined the reference space. Since all images were approximately the same size, the total reference space was equal to the number of images times the size of an image. This time, instead of counting points, intersections (I) were counted when the test lines crossed the surface of granules. Again, a large enough number of intersections had to be counted so that the sampling error was less than 10%. The surface density of the granules (S_V), defined as the total surface area of granules per total reference space volume, could be calculated using equation 5 (30).

$$S_V = 2 \times \Sigma I_G / \Sigma L \qquad (5)$$

where ΣI_G is the number of intersections of granules with test lines, summed over all images, and ΣL is the total length of test lines summed over all images. Again, the length had to be corrected for magnification. Note that the units for S_V are length^{-1} (e.g., μm^{-1}). The derivation of this equation has been described by Elias et al. (11; also see). Recall that V_V (V_{obj}/V_{ref}) is the total volume of observed cell profiles in the total reference space, which in our case was obtained from the same images. Therefore, dividing S_V by V_V gives the total surface area of granules in a unit volume of cells. The total surface area of granules in one cell (S_G) can be obtained using the following equation.

$$S_G = (S_V/V_V) \times V_{CP} \qquad (6)$$

Again, this analysis was applied to images of all our samples.

Measurement of size distribution of cell and granule profiles on 2-D images. For all wild-type samples, the major and minor axes of all cell and granule profiles were measured for images recorded at the same low magnification (primary magnification, ×3,000) so that a large field of cells could be sampled. Measurements were made by using the Scion Image for Windows software from Scion Corporation. These measurements were confirmed by random manual measurements with rulers.

RESULTS

Transition of cells from nutrient-rich medium (TSB) to PHB$_P$. Current work on PHB has been mostly focused on studying the phenotype of microorganisms grown under con-

ditions in which the maximum number of PHB granules is produced. A typical TEM picture shows a cell that is full of large granules (e.g., a cell after 24 h in PHB$_P$ [Fig. 3D]). However, the fate of *W. eutropha* cells during the initial stage of PHB production has not, to our knowledge, been determined. We were interested in using TEM to observe cells at the early stages. *W. eutropha* is typically grown in TSB rich medium for 24 h to minimize the amount of PHB in cells used to inoculate PHB$_P$. Ideally, the starting culture would contain cells in the early stationary phase and would contain no PHB so that the PHB production in PHB$_P$ could be monitored from the very beginning. However, in our hands, such growth conditions have not been identified yet. At 24 h in TSB, *W. eutropha* contains a small amount of PHB ($<10\%$ of cell dry weight) (38). Cells grown under these conditions were thus chosen to serve as the inoculum. Images of cells at 24 h in TSB and at an early time (2.5 h) in PHB$_P$ are shown in Fig. 4 and revealed surprising results. Upon a switch into PHB$_P$, the *W. eutropha* cell size increased two- to threefold (Table 1, compare A_{CP}/N_{CP} values for TSB at 24 h and for PHB$_P$ at 2.5 h). The increased size could have been associated with cell division, since the cells were transferred from nutrient-depleted TSB at 24 h, when most of the cells were no longer dividing, to PHB$_P$, which contained a nitrogen source at a concentration of 0.01% and initially allowed cell growth. A typical recently divided rod-shaped cell (e.g., *Escherichia coli*) elongates with little or no increase in girth until it reaches approximately twice its original size and then separates into two cells that are nearly equal in size (17). Alternatively, an increase in cell volume could be related to the ability of cells to sense nitrogen nutrient limitation. Thus, the increased cell size may be a regulatory mechanism required to maximize the cell's capacity for granule storage. Support for this alternative explanation was provided by the observation that the average cell volume at 2.5 h in PHB$_P$ was still substantially larger than that at 4 h in TSB in which the cells were also dividing (Table 1). The basis for cell volume increase requires further investigation.

Kinetics of wild-type *W. eutropha*: unusual mediation elements accommodating small granules at early times. Models in the literature for granule formation suggest that granules may arise through physical association of PHB oligomers forming micelle-like structures (Fig. 1) (12) or by budding off the plasma membrane, resulting in a granule covered with a monolayer of lipid (Fig. 2) (32). TEM may allow a distinction between these models, as in the former case the granules may be uniformly dispersed in the cytoplasm and in the latter case the nascent granules should be adjacent to the inner leaflet of the plasma membrane of the cell. In this study wild-type *W. eutropha* was examined in PHB$_P$ as a function of time, and images of the time course are shown in Fig. 3. At the early times (2.5 and 5 h), striking dark-stained structures or mediation elements (0.4 to 0.5 µm) were observed near the center of the cross section of many cells (Fig. 3A and B and 4) or along a longitudinal strip in the center of the cells (Fig. 5 and 6A). The location of these dark-stained mediation elements at the center of the cells was confirmed by images from serial sections (data not shown). These mediation elements are believed to be unique to *W. eutropha* studied under PHB$_P$ conditions since *E. coli* cells (which closely resemble *W. eutropha* cells) to our knowledge do not show such mediation elements under normal
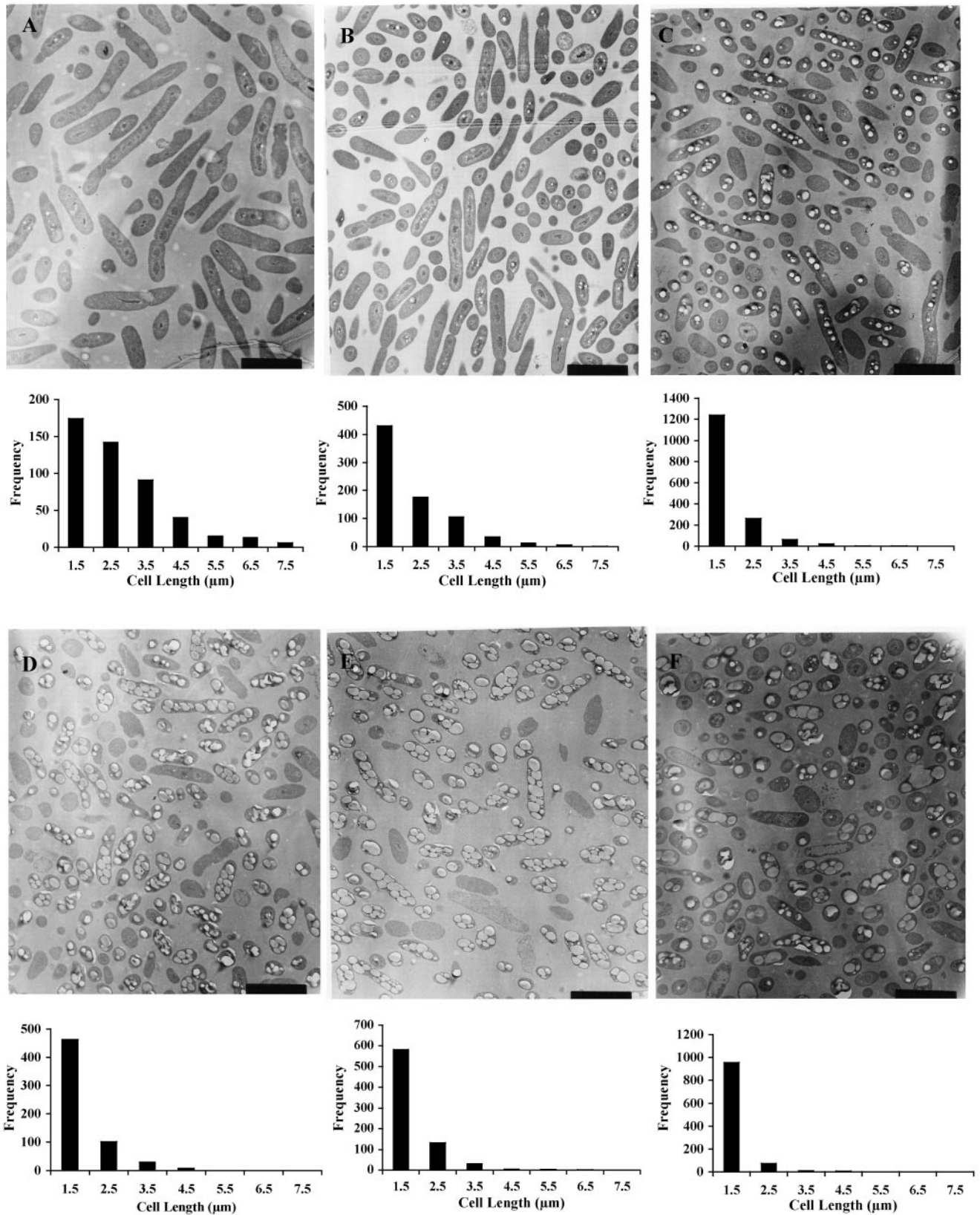
FIG. 3. TEM images of wild-type *W. eutropha* during growth in PHB$_P$ and PHB$_U$. (A) PHB$_P$ at 2.5 h; (B) PHB$_P$ at 5 h; (C) PHB$_P$ at 9 h; (D) PHB$_P$ at 24 h; (E) PHB$_P$ at 73 h; (F) PHB$_U$ at 48 h. All images were recorded at the same magnification (bars, 3 μm). The changes in cell size for the samples are reflected by the histograms below the images. The histograms indicate the size distribution of cell profiles (obtained by measuring the major axis of all cell profiles). Images other than the ones shown were also used for this analysis.
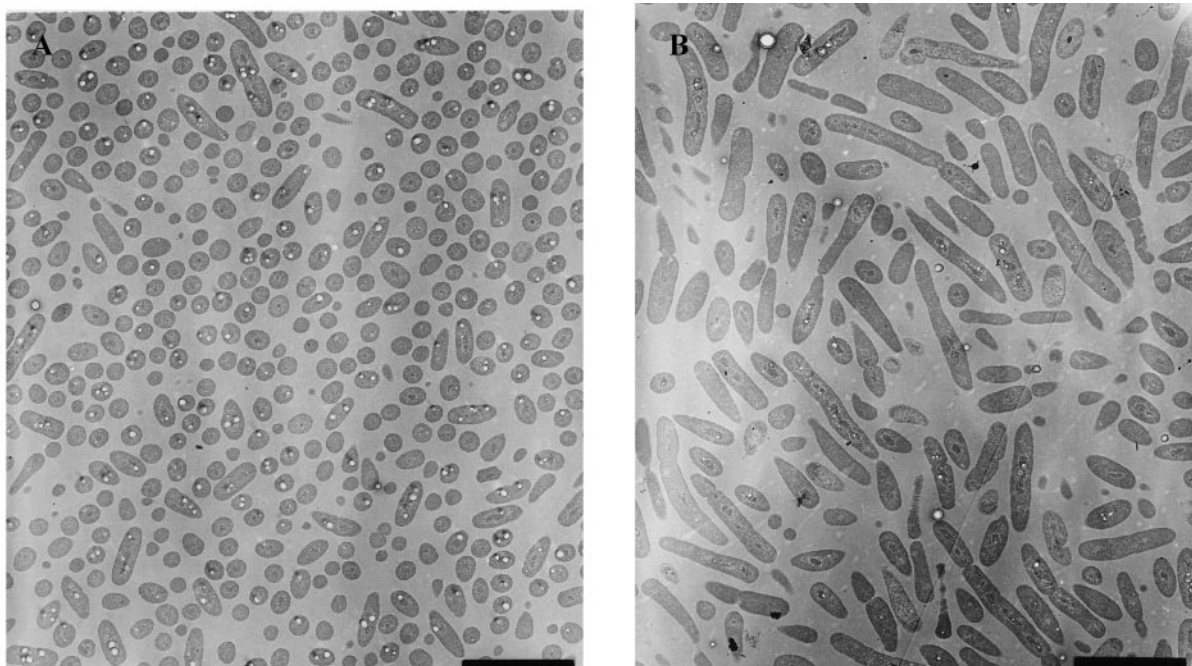
FIG. 4. TEM images of wild-type *W. eutropha* grown in TSB for 24 h (A) and wild-type *W. eutropha* grown in PHB$_P$ for 2.5 h after 24 h in TSB (B). The two images are the same magnification (bars, 4.5 μm).

growth conditions when they are fixed and stained under similar conditions and analyzed by TEM (13, 18). Of great interest is the finding that very small PHB granules (Fig. 5) localize around these dark-stained mediation elements. Examination of many images containing thousands of cells gave no evidence that PHB granules bud from the cell membrane or are dispersed randomly within the cytoplasm. As the cells continued to grow in PHB$_P$ from 5 to 73 h, the dark mediation elements gradually disappeared or became obscured by the increased size of the granules (Fig. 3 and 6). Notice that the size of the granules increased from 9 to 24 h in PHB$_P$, until the entire cell was filled with granules.

The mediation elements have also been observed in a *W. eutropha* strain in which the class I synthase gene was replaced with D302A-PhaCPhaE (class III synthase) from *Allochromatium vinosum*. Although this organism was grown in PHB$_P$ for
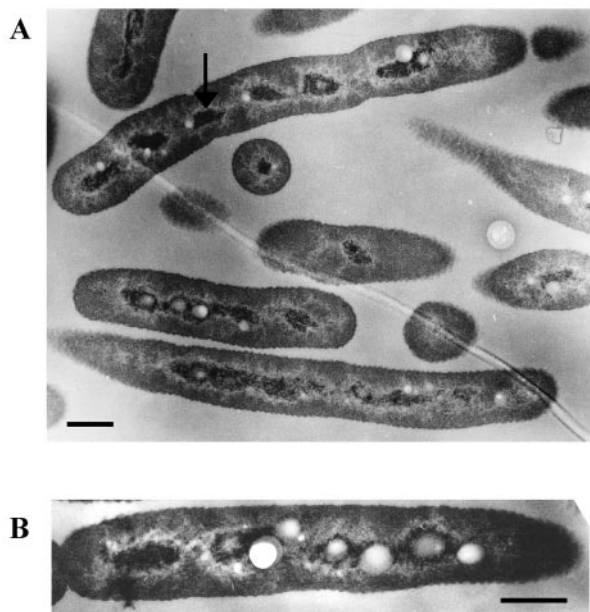

FIG. 5. TEM images of wild-type *W. eutropha* at 2.5 h in PHB$_P$. Nascent granules are localized on dark-stained mediation elements near the center of the cell. Bars, 0.5 μm. (A) The arrow indicates a dark-stained mediation element. (B) Cell at higher magnification.
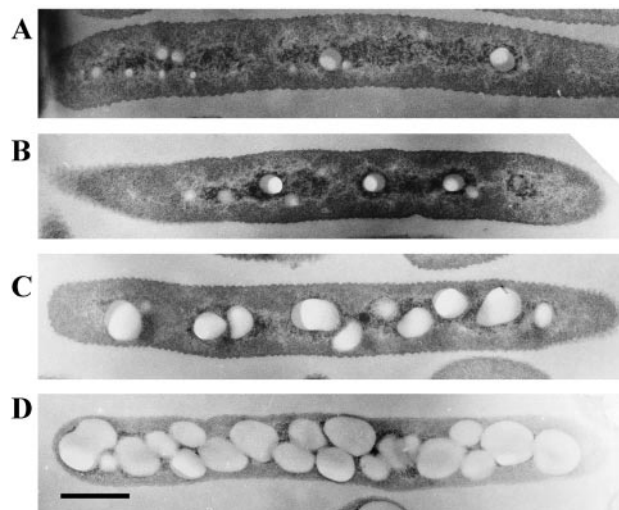

FIG. 6. TEM images of wild-type *W. eutropha* in PHB$_P$ at 2.5 h (A), 5 h (B), 9 h (C), and 24 h (D), showing the "disappearance" of the dark-stained mediation elements. Bar, 0.5 μm.
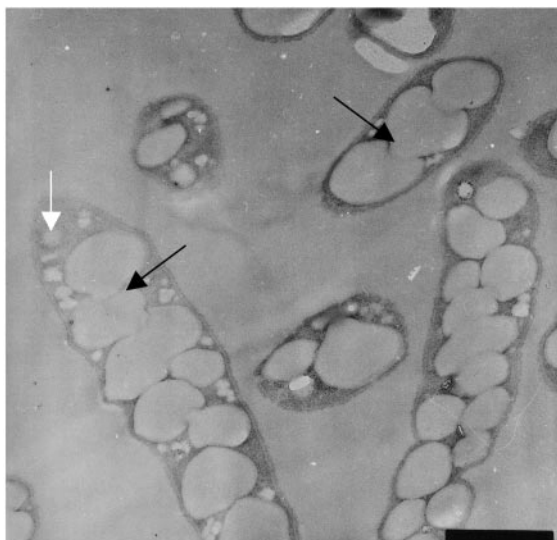
FIG. 7. TEM image of *W. eutropha* at 73 h in PHB$_P$. Significant granule coalescence (black arrows) was observed. In addition, small granules of unknown composition (white arrow) are present. Bar, 0.8 μm.
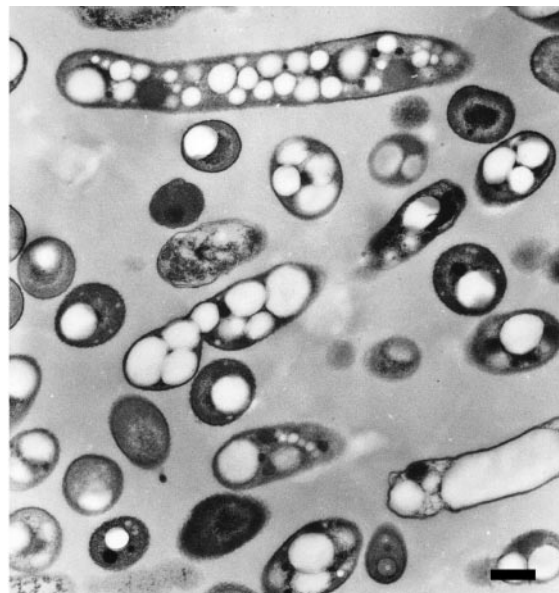

FIG. 8. TEM image of *W. eutropha* at 48 h in PHB$_U$. There seemed to be different populations of cells. Some cells contained a high number of smaller granules (compared to those at 24 h in PHB$_P$), while others contained a few large granules. Bar, 0.5 μm.

24 h (compare with the wild-type strain in Fig. 3D), only small granules were observed to accumulate since the mutant was defective in the ability to elongate a polymer (35). The mediation elements were again seen near the center of the cross sections of cells, where the small granules were found.

The observation of these mediation elements with attached granules is intriguing. However, it should be kept in mind that the cells were cross-linked with glutaraldehyde and paraformaldehyde, fixed and stained with osmium tetroxide and uranyl acetate, and extensively dehydrated with ethanol. A variety of additional methods to scrutinize these interesting mediation elements to ensure their relationship to granule formation will be the focus of future experiments.

As shown in Fig. 3B, C, and D and 6, a significant amount of PHB was produced from 5 to 9 h and from 9 to 24 h in PHB$_P$. Cells containing as many as 18 to ~25 granules per cell were occasionally observed in our images at 24 h. At 73 h, significant coalescence of granules was observed, as shown in Fig. 7. Also of interest is the appearance of small white inclusions near the edge of the cell membrane (Fig. 7). The identity of these inclusions is uncertain, and their origin is also unknown.

When the cells were transferred into PHB$_U$ after 73 h in PHB$_P$, the size of the *W. eutropha* cells decreased by 48 h (Fig. 3F). Furthermore, at this time, the size and number of granules were much more heterogeneous than they were in PHB$_P$ (Fig. 3F and 8). The observation of granules at this time agrees with our previous PHB quantitation obtained using the crotonic acid assay, which showed that ~40% of PHB based on the cell dry weight remained at 48 h and thereafter (38). The TEM photographs clearly established for the first time that almost all of this PHB was inside the cell and was not extracellular. The reason for the cell's inability to completely degrade PHB under these utilization conditions is not understood at present.

Changes in cell volume during PHB production and utilization. Knowledge of the concentration of proteins involved in

PHB homeostasis and how the proteins change during PHB production and utilization is an essential component for understanding this process. Calculation of the in vivo concentration of proteins requires knowledge of the cell size at the time of interest. The TEM photographs in Fig. 3 and 4 did not reveal cell volume changes under PHB production and utilization conditions by direct examination. Since TEM pictures present essentially flat profiles of cells obtained from random cuts through an embedded sample, the size of a cell profile is not representative of the size of the cell from which it arose. The method that has allowed quantitation of changes in cell volume from 2-D images such as those shown in Fig. 3 is the theoretically unbiased stereology method (10, 26). After measurements of the 2-D images are taken, parameters from these measurements can be extrapolated to three-dimensional space, regardless of the shape and size of the object of interest. This estimation method has been used widely in geology, material science, and neurosciences and in the study of many biological tissues. Although stereology has not been used much in the study of bacterial cells, TEM images of bacteria are ideal for analysis by this method, since the cells in sections are embedded randomly and they are isotropic (having no preference in orientation). Stereology is practiced by superimposing line and point patterns on flat images of thin sections, from which the component(s) of interest can be quantified. Counted points and measured line segments are tabulated and entered into basic, assumption-free formulas, as described in Materials and Methods. Since all cell samples are fixed by the same method, the effect of fixation on cell and granule size is assumed to be the same for all samples. This is, however, a caveat, since the amount of PHB differs in each sample, which could differentially affect fixation.

Using the point-counting method (see Materials and Methods), the total area of cell profiles (A_{CP}) on all images was
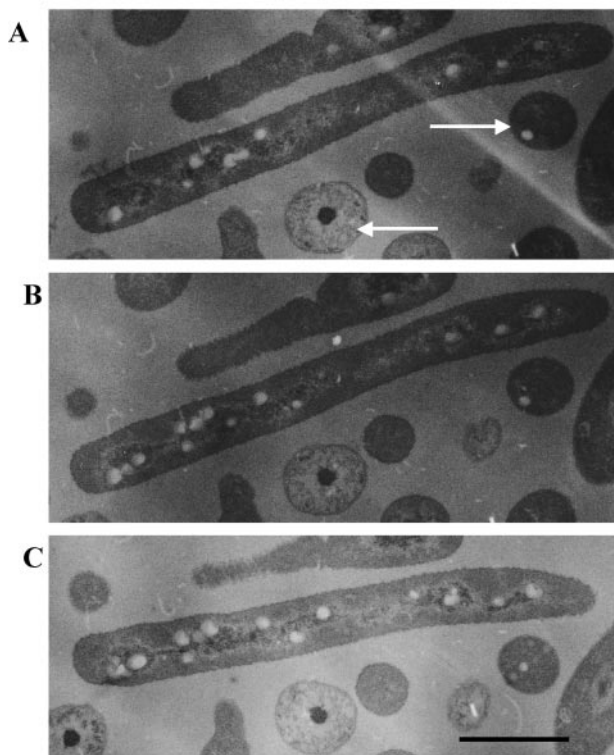
FIG. 9. TEM images of consecutive serial sections (A→B→C) of the sample at 5 h in PHB$_P$. The longest cell profile appears to result from a cell that is lying parallel to the plane of the sectioning knife, since its position does not change relative to the other two cell profiles (arrows), which seem to result from cells that were lying perpendicular to the place of section. Since the length of the long cell profile does not change from panel A to panel B, this length represents the actual length of the cell. Notice that the cell length in panel C is less. These images also reveal that the size of the granules is fairly uniform. Bar, 1 μm.

TABLE 2. Estimated average cell volumes calculated using the average length of the longest cell profiles (~4% of the total cell profiles measured) at each time and average widths of all cell profiles in images used to measure the length of the cell profiles[a]

Sample	No. of cell profiles measured	Width (μm)[b]	Avg cell vol (μm³)
PHB$_P$, 2.5 h	482	0.75 ± 0.015	2.4[c]
PHB$_P$, 5 h	768	0.69 ± 0.014	1.7[c]
PHB$_P$, 9 h	1,596	0.66 ± 0.007	1.2
PHB$_P$, 24 h	600	0.68 ± 0.011	1.3
PHB$_P$, 73 h	754	0.74 ± 0.011	1.5

[a] See the histograms in Fig. 3. The formula for the volume of a cylinder was used for calculation.
[b] Average ± 95% confidence interval.
[c] Volume of cells on the verge of cell devision.

calculated for samples harvested at defined times during cultivation. As implied in equation 1 (see Materials and Methods), A_{CP} is directly proportional to the size and number of cell profiles (N_{CP}) on all images, and the larger and the greater the number of cell profiles, the greater the number of hit points (P) with the test probe. While the size of cell profiles and its change from sample to sample were a result of the experimental testing conditions, the number of cell profiles on images was not since cells were randomly embedded and images were recorded randomly. Therefore, in order to be able to use A_{CP} for comparison purposes from sample to sample, A_{CP} must be normalized by the number of cell profiles (hence, A_{CP}/N_{CP}). The change in cell volume among the samples is directly reflected in this assumption-free (no assumption concerning the shape of the cell) value of A_{CP}/N_{CP}, as shown in Table 1. According to the Delesse principle, the area of cell profiles in a reference space (A_A) is equivalent to the volume of those profiles in the same reference space (V_V). Therefore, knowing the actual average volume of cells at one time allows calculation of the average volume of cells at other times, as described in Materials and Methods.

In order to obtain the actual average volume of cells at one time, images from serial sections of cells are required. We

chose to examine cells in PHB$_P$ at 5 h. An example of typical serial sections is shown in Fig. 9. The average cell volume analysis for this time was complicated by cell growth and division. We chose the longest cell profiles from images of serial sections, and thus, the volume determined represents the population of cells just before cell division. Assuming the cells divided equally, the volume of each daughter cell is approximately one-half the volume of the original cell. The determination of the length and width of the cell profiles from these sections is described in Materials and Methods. The average volume of a cell can be calculated using the volume equation for a cylinder, assuming that *W. eutropha* is rod shaped. The average cell volume at 5 h in PHB$_P$ using the longest cell profiles was estimated to be 1.8 μm³ or 1.8×10^{-15} liter (Table 1). This value, chosen since most of the cells in TEM images and measured were in the cell division process (Fig. 3A and B and 4B), allowed estimation of the average cell volume of the samples taken at other times. The results are summarized in Table 1 and were verified by a second approach, as described below. The largest change in volume was between TSB at 24 h and PHB$_P$ at 2.5 h. This change reflected cell doubling. However, it was sufficiently large that an additional contribution to size might have resulted from sensing nitrogen limitation and preparing for PHB storage.

The trends observed in cell volume change as a function of time in PHB$_P$ were verified independently by measuring the size distribution of cell profiles on images recorded at a low magnification (negatives were at a magnification of ×3,000) so that a large number of cells was examined at each time. A population of large cells should give a higher frequency of long and wide cell profiles than a population of small cells if all cells are randomly embedded and examined. The major and minor axes of hundreds to thousands of cell profiles, regardless of shape and size, were measured for PHB$_P$ at 2.5, 5, 9, 24, and 73 h. Graphic representations of the profile frequency for cell length are shown in the histograms in Fig. 3. Less variation was observed in width, and, therefore, only the average width is reported here (Table 2). The average length of the cells decreased as a function of time, while the width decreased slightly from 2.5 to 9 h and then increased slightly. As a result, the volume of the cell decreased from 2.5 to 9 h and then gradually increased from 9 to 73 h in PHB$_P$, a trend similar to that measured by stereology (Table 1). In addition, using the average length of the longest cell profiles (usually ~4% of the total

number of cell profiles measured) and the average width (Table 2) from images obtained at each of these times, the average volume of cells calculated using the equation for the volume of a cylinder (Table 2) is very similar to the volumes obtained from stereology. Note that the longest cell profile in PHB$_P$ at 9, 24, and 73 h should represent the actual length of the cell population, since cells were no longer dividing, as indicated by the constant dry cell weight (with the weight of PHB subtracted) at these times (data not shown). Thus, it is appropriate to assume that all cells are a uniform size at these times.

The average cell volumes in TSB conditions were also measured for the 4- and 24-h samples using stereology. Again, a range of volumes is reported for the 4-h point in Table 1 due to cell division. From 12 to 24 h in TSB, the mass of the cell (with the weight of PHB subtracted) increased by only ~30% (data not shown), indicating that most of the cells were entering the stationary phase. Therefore, the average cell volume determined for TSB at 24 h is close to that of a single cell.

Changes in surface area of granules in wild-type *W. eutropha* during growth in PHB$_P$. Another piece of information that can contribute significantly to our understanding of PHB biosynthesis and degradation in *W. eutropha* is the amount of each protein covering the surface of granules. Immunogold labeling studies using antibodies to the synthase (PhaC) and the phasin (PhaP) and TEM analysis revealed that these two proteins are on the surface of granules (15, 27). The large amounts of PhaP produced (estimated to be 3 to 5% of the total amount of protein present under maximum PHB production conditions) were the basis for the proposal that the granules are mostly covered with PhaP (31). Substantial coverage, however, is not apparent in a TEM image (27). Immunogold labeling and TEM imaging also suggested that there was very low coverage of the granule surface by PhaC. No quantitation of the surface coverage has been reported previously. In order to calculate the amount of protein covering granule surfaces, the total surface area of granules per cell (S_G) needs to be determined at each time, as does the amount of each protein of interest. Again, stereology has been used to solve this problem. As shown in Fig. 3 and 4, the granules in TSB at 4 h (not shown) and 24 h and in PHB$_P$ at 2.5, 5, and 9 h appeared to be spherical. However, the shape of the granules at the later times was altered due to crowding and granule fusion. The beauty of the stereological method is that S_G can be derived without knowing the shape and the number of the granules per cell since S_G is a function of the number of intersections between granule surfaces and test lines and the length of the test line probes. The value of S_G for each time is also reported in Table 1. Note that a range of S_G values are reported for the TSB sample at 4 h, which correspond to the range of cell volumes reported. S_G is not reported for the 2.5- and 5-h samples from PHB$_P$ since the granules were too small and not defined sufficiently to be quantitated.

The granules in TSB at 4 and 24 h appeared to be roughly spherical, and coalescence was not observed. Therefore, an alternative method was used to estimate S_G, providing confirmation of the results obtained from the analysis using stereology. The diameter of every single-granule profile on images containing 500 to 600 granules was measured for each sample. These granule profile diameters were averaged to give apparent granule diameters ($\bar{d}$) of 0.28 ± 0.02 µm and 0.19 ± 0.004

µm (average ± 95% confidence interval) for 4- and 24-h TSB samples, respectively. The $\bar{d}$ values were necessarily lower than the actual granule diameter ($\bar{D}$) since cross sectioning intersects granules at random. $\bar{D}$ and $\bar{d}$ are related by equation 7 (10).

$$\bar{D} = (4/\pi) \times \bar{d} \tag{7}$$

The calculated $\bar{D}$ values for 4- and 24-h TSB samples were 0.36 and 0.24 µm, respectively, if all granules were the same size. Note that this assumption is more suitable for the 24-h sample than for the 4-h sample since the granules appeared to be more heterogeneous at the early time, as revealed in the serial sections of both samples (data not shown). The surface area of a granule (S) can be calculated by using the formula for a sphere, $S = \pi\bar{D}^2$. Since there are approximately 2.5 to 5 granules per cell in TSB at 4 h (depending on the choice of average cell volume) and 5 granules per cell in TSB at 24 h (34), the total surface areas of granules per cell in TSB at 4 and 24 h were calculated to be 1 to 2 µm^2 and 0.9 µm^2, respectively. These values are very close to those obtained through stereology (Table 1).

DISCUSSION

Two models of PHB granule formation have been put forth in the current PHB literature: the micelle model (Fig. 1) and the budding model (Fig. 2). Both models account for the established location of the synthase and phasin on the surface of the granule. Earlier TEM studies revealing membrane-like material surrounding granules in intact cells (3, 9, 19, 36) or isolated granules (23, 25) also provided the basis for the budding model. We therefore studied the early stages of granule formation in *W. eutropha* under nitrogen limitation growth conditions with the hope of obtaining insight into the mechanism of this process. The cells examined by TEM were fixed, stained, and dehydrated. In the analysis that followed we assumed that the observations made were not an artifact of the fixation method. Instead of observing granules randomly distributed in the cytoplasm and close to the inner cell membrane, as expected from Fig. 1 and 2, respectively, we found that nascent granules arose from only the center of the cell. In addition, pronounced dark-stained mediation elements were also found at the center of the cells, and it is to these mediation elements that granules appeared to be localized. As cultivation in PHB$_P$ continued, the granules grew uniformly, and the dark mediation elements were no longer observed.

The molecular identities of these mediation elements are currently unknown. Osmium tetroxide and uranyl acetate both serve as fixatives and stains for lipids, proteins, nucleic acids, and other cellular structures (4). The mechanism of staining is not well understood for either reagent. As a result of the nonspecific staining by both reagents, the dark-stained mediation elements could be any of the candidates listed above or other deposits that reacted with the staining reagents. Staining with more specific reagents may help in elucidating the composition of the mediation elements. Localization of nascent granules close to the unknown mediation elements has led us to propose a new model for PHB granule formation: the mediation elements could serve as scaffolds, providing sites for the

synthase to initiate granule formation. Subsequent to granule initiation, a number of possibilities for the fate of the scaffold have been considered. The first possibility is that the scaffold (0.4 to 0.5 μm) becomes covered with granules. The second is that at some stage in granule growth, the scaffold is degraded. A third possibility is that the material that composes the scaffolds could be distributed over the surface of the granule as it is being made. In any of these scenarios, the mediation elements would not be observed at the late stage of PHB biosynthesis. The concept of scaffolds has been exemplified by the cellulosome, the multicomponent, multienzyme complex from anaerobic cellulolytic bacteria that is used to degrade plant cell wall polysaccharides (2, 8, 21). The main component of the cellulosome is a multienzyme integrating protein unit called scaffoldin. Scaffoldin contains several cohesion domains, which recruit enzymes that play roles in cellulose degradation and contain a "dockerin" domain. The cohesion-dockerin interaction allows the scaffoldin to organize the various cellulolytic components into a complex, which then allows all these enzymes to work efficiently and synergistically. The existence of this "machinery" for cellulose degradation suggests that there could be a similar complex for orchestrating the proteins involved in PHB biosynthesis and degradation. Recently, Dennis et al. observed large structures on the surface of PHB-containing granules from *W. eutropha* cells using atomic force microscopy. They proposed that these structures might serve as synthesis-degradation centers (7). Isolation and identification of the dark-stained mediation elements observed by TEM, therefore, are important for verifying our new model and unraveling the process of PHB formation in vivo.

In this paper, we also report the estimated average cell volume and total surface area of granules per cell for *W. eutropha* H16 cells grown in nutrient-rich TSB and in PHB$_P$ as determined by stereological analysis of TEM images. Once again, the assumption was made that fixation of the cells did not affect the sizes of the cells or the granules. The growth conditions used in this study have been widely used in the PHB field, and therefore, these new parameters of cells should be useful to other workers interested in understanding the PHB homeostasis. Recently, our laboratory has carried out a series of studies to determine the amount of proteins involved in PHB homeostasis in *W. eutropha* under these growth conditions using quantitative Western analyses (34). The results of the Western analyses, together with the cell volume and granule surface area calculated in this study, have provided new information concerning the homeostasis of PHB.

REFERENCES

1. **Anderson, A. J., and E. A. Dawes.** 1990. Occurrence, metabolism, metabolic role, and industrial uses of bacterial polyhydroxyalkanoates. Microbiol. Rev. **54:**450–472.
2. **Bayer, E. A., J. P. Belaich, Y. Shoham, and R. Lamed.** 2004. The cellulosomes: multienzyme machines for degradation of plant cell wall polysaccharides. Annu. Rev. Microbiol. **58:**521–554.
3. **Boatman, E. S.** 1964. Observations on the fine structure of spheroplasts of *Rhodospirillum rubrum*. J. Cell Biol. **20:**297–311.
4. **Bozzola, J. J., and L. D. Russell.** 1999. Electron microscopy. Jones and Bartlett Publishers, Boston, Mass.
5. **Cavalieri, B.** 1966. Geometria degli indivisibili. Unione Tipografico—Editrice Torinese, Turin, Italy. [Reprint of Geometria indivisibilibus continuorum. Typis Clementis Ferronij, Bononi, 1635.]
6. **Delesse, A.** 1848. Procede mecanique pour determiner la composition des roches. Ann. Mines. **13:**379.
7. **Dennis, D., C. Liebig, T. Holley, K. S. Thomas, A. Khosla, D. Wilson, and B. Augustine.** 2003. Preliminary analysis of polyhydroxyalkanoate inclusions using atomic force microscopy. FEMS Microbiol. Lett. **226:**113–119.
8. **Devillard, E., D. B. Goodheart, S. K. Karnati, E. A. Bayer, R. Lamed, J. Miron, K. E. Nelson, and M. Morrison.** 2004. *Ruminococcus albus* 8 mutants defective in cellulose degradation are deficient in two processive endocellulases, Cel48A and Cel9B, both of which possess a novel modular architecture. J. Bacteriol. **186:**136–145.
9. **Dunlop, W. F., and A. W. Robards.** 1973. Ultrastructural study of poly-β-hydroxybutyrate granules from *Bacillus cereus*. J. Bacteriol. **114:**1271–1280.
10. **Elias, H., and D. M. Hyde.** 1983. A guide to practical stereology. Karger, Basel, Switzerland.
11. **Elias, H., A. Hennig, and D. E. Schwartz.** 1971. Stereology: applications to biomedical research. Physiol. Rev. **51:**158–200.
12. **Ellar, D., D. G. Lundgren, K. Okamura, and R. H. Marchessault.** 1968. Morphology of poly-beta-hydroxybutyrate granules. J. Mol. Biol. **35:**489–502.
13. **Fuller, R., and D. W. Lovelock.** 1976. Microbial ultrastructure: the use of the electron microscope. The Society for Applied Bacteriology Technical Series. Academic Press, London, United Kingdom.
14. **Gerngross, T. U., K. D. Snell, O. P. Peoples, A. J. Sinskey, E. Cushai, S. Masamune, and J. Stubbe.** 1994. Overexpression and purification of the soluble polyhydroxyalkanoate synthase from *Alcaligenes eutrophus*: evidence for a required posttranslational modification for catalytic activity. Biochemistry **33:**9311–9320.
15. **Gerngross, T. U., P. Reilly, J. Stubbe, A. J. Sinskey, and O. P. Peoples.** 1993. Immunocytochemical analysis of poly-β-hydroxybutyrate (PHB) synthase in *Alcaligenes eutrophus* H16: localization of the synthase enzyme at the surface of PHB granules. J. Bacteriol. **175:**5289–5293.
16. **Glagolev, A. A.** 1933. On the geometrical methods of quantitative mineralogic analysis of rocks. Trans. Inst. Econ. Mineral. Metallurg. **59:**1.
17. **Ingraham, J. L., O. Maaloe, and F. C. Neidhardt.** 1983. Growth of the bacterial cell. Sinauer Associates, Inc., Sunderland, Mass.
18. **Iterson, W. V.** 1984. Inner structures of bacteria. Van Nostrand Reinhold Company Inc., New York, N.Y.
19. **Jensen, T. E., and L. M. Sicko.** 1971. Fine structure of poly-beta-hydroxybutyric acid granules in a blue-green alga, *Chlorogloea fritschii*. J. Bacteriol. **106:**683–686.
20. **Kobayashi, T., M. Shiraki, T. Abe, A. Sugiyama, and T. Saito.** 2003. Purification and properties of an intracellular 3-hydroxybutyrate-oligomer hydrolase (PhaZ2) in *Ralstonia eutropha* H16 and its identification as a novel intracellular poly(3-hydroxybutyrate) depolymerase. J. Bacteriol. **185:**3485–3490.
21. **Kosugi, A., Y. Amano, K. Murashima, and R. H. Doi.** 2004. Hydrophilic domains of scaffolding protein CbpA promote glycosyl hydrolase activity and localization of cellulosomes to the cell surface of *Clostridium cellulovorans*. J. Bacteriol. **186:**6351–6359.
22. **Liebergesell, M., K. Sonomoto, M. Madkour, F. Mayer, and A. Steinbuchel.** 1994. Purification and characterization of the poly(hydroxyalkanoic acid) synthase from *Chromatium vinosum* and localization of the enzyme at the surface of poly(hydroxyalkanoic acid) granules. Eur. J. Biochem. **226:**71–80.
23. **Lundgren, D. G., R. M. Pfister, and J. M. Merrick.** 1964. Structure of poly-beta-hydroxybutyric acid granules. J. Gen. Microbiol. **34:**441–446.
24. **Maehara, A., S. Taguchi, T. Nishiyama, T. Yamane, and Y. Doi.** 2002. A repressor protein, PhaR, regulates polyhydroxyalkanoate (PHA) synthesis via its direct interaction with PHA. J. Bacteriol. **184:**3992–4002.
25. **Mayer, F., M. Madkour, U. Pieper-Furst, R. Wieczorek, M. Liebergesell, and A. Steinbuchel.** 1996. Electron microscopic observations on the macromolecular organization of the boundary layer of bacterial PHA inclusion bodies. J. Gen. Appl. Microbiol. **42:**445–455.
26. **Mouton, P. R.** 2002. Principles and practices of unbiased stereology: an introduction for bioscientists. The Johns Hopkins University Press, Baltimore, Md.
27. **Potter, M., M. H. Madkour, F. Mayer, and A. Steinbuchel.** 2002. Regulation of phasin expression and polyhydroxyalkanoate (PHA) granule formation in *Ralstonia eutropha* H16. Microbiology **148:**2413–2426.

28. **Rehm, B. H., and A. Steinbüchel.** 1999. Biochemical and genetic analysis of PHA synthases and other proteins required for PHA synthesis. Int. J. Biol. Macromol. **25:**3–19.
29. **Saegusa, H., M. Shiraki, C. Kanai, and T. Saito.** 2001. Cloning of an intracellular poly[D(−)-3-hydroxybutyrate] depolymerase gene from *Ralstonia eutropha* H16 and characterization of the gene product. J. Bacteriol. **183:**94–100.
30. **Smith, C. S., and L. Guttman.** 1953. Measurement of internal boundaries in three-dimensional structures by random sectioning. Trans. AIME **197:**81–111.
31. **Steinbüchel, A., K. Aerts, W. Babel, C. Föllner, M. Liebergesell, M. H. Madkour, F. Mayer, U. Pieper-Fürst, A. Pries, H. Valentin, and R. Wieczorek.** 1995. Considerations on the structure and biochemistry of bacterial polyhydroxyalkanoic acid inclusions. Can. J. Microbiol. **41**(Suppl. 1)**:**94–105.
32. **Stubbe, J., and J. Tian.** 2003. Polyhydroxyalkanoate (PHA) homeostasis: the role of PHA synthase. Nat. Prod. Rep. **20:**445–457.
33. **Thomson, W. R.** 1930. Quantitative microscopic analysis. J. Geol. **38:**193.
34. **Tian, J., A. He, A. G. Lawrence, P. Liu, N. Watson, A. J. Sinskey, and J. Stubbe.** 2005. Analysis of transient polyhydroxybutyrate production in *Wautersia eutropha* H16 by quantitative Western analysis and transmission electron microscopy. J. Bacteriol. **187:**3825–3832.
35. **Tian, J., A. J. Sinskey, and J. Stubbe.** Detection of intermediates from the polymerization reaction catalyzed by a D302A mutant of class III polyhydroxyalkanoate (PHA) synthase. Biochemistry, in press.
36. **Wang, W. S., and D. G. Lundgren.** 1969. Poly-beta-hydroxybutyrate in the chemolithotrophic bacterium *Ferrobacillus ferrooxidans.* J. Bacteriol. **97:**947–950.
37. **York, G. M., J. Stubbe, and A. J. Sinskey.** 2002. The *Ralstonia eutropha* PhaR protein couples synthesis of the PhaP phasin to the presence of polyhydroxybutyrate in cells and promotes polyhydroxybutyrate production. J. Bacteriol. **184:**59–66.
38. **York, G. M., J. Lupberger, J. Tian, A. G. Lawrence, J. Stubbe, and A. J. Sinskey.** 2003. *Ralstonia eutropha* H16 encodes two and possibly three intracellular poly[D-(−)-3-hydroxybutyrate] depolymerase genes. J. Bacteriol. **185:**3788–3794.